Functionalization of the C_{20} fullerene by pyridine and pyrimidine: A theoretical study

Mousa Soleymani*, Hossein Dashti Khavidaki

Department of Chemistry, Faculty of Basic Science, Ayatollah Boroujerdi University, Boroujerd 69199-69411, Iran

Abstract

A theoretical study at the levels of CAM-B3LYP and MP2 was reported, with the aim of understanding the possibility of functionalization of the C_{20} fullerene with pyridine and pyrimidine via a cycloaddition reaction. For this purpose, several [2+2] and [4+2] cycloaddition reactions were considered between C_{20} and pyridine or pyrimidine, and their thermodynamic and kinetic parameters were calculated. The results indicated that those [4+2] cycloaddition reactions are favorable ones in which the fullerene plays the role of a dienophile. It was also found that a [4+2] reaction path in which it takes place *via* the formation of two new C–C bonds between two fragments, C_{20} and heterocycle, is more favorable than that occurring *via* the formation of two different bonds, C-C and C–N. The calculation of global electron density transfer (GEDT) and molecular electrostatic potential (MESP) map revealed that the transition states are relatively polar and the C_{20} fullerene acts as an electron acceptor. Determination of Frontier Effective-for-Reaction Molecular Orbitals (FERMOs) relevant to pyridine and pyrimidine satisfactorily described the reactivity of different active sites of pyridine and pyrimidine. Finally, the calculation of the reactions synchronicity showed that the reactions are relatively synchronous.

Keywords: C_{20} fullerene; pyridine; pyrimidine; GEDT; FERMO; functionalization.

Introduction

Fullerenes are one class of carbon nanostructures that contain conjugated π-bonds. These low-dimensional structures play an important role in the development of nanotechnology. The most popular fullerene, C_{60}, also known as buckminsterfullerene, was first discovered in 1985 [1]. After the discovery of the C_{60} fullerene, several other carbon clusters were synthesized, in spherical or ellipsoidal structure and, also, their chemical and physical properties were investigated both experimentally and theoretically [2]. The smallest possible fullerene is C_{20}, which was first synthesized from its perhydrogenated form, $C_{20}H_{20}$, in the gas phase [3]. The reactivity of C_{20} is more than the other fullerenes, which can be attributed to its non-spherical aromaticity, low energy gap and inherent instability [4].

In recent years, extensive researches which have been performed on the fullerenes and their derivatives have led to the development of medicine and nanotechnology [5-8]. These nanoscale

*Corresponding author: Mousa Soleymani
Tel: +98 (66) 42468320, Fax: +98 (66) 42468322
E-mail: m.soleymani@abru.ac.ir

materials have low polarity, and consequently, their applications are limited in aqueous media. To eliminate these drawbacks, some successful attempts have been done to improve the properties of fullerenes. The functionalization is known as a suitable protocol to modify the properties of fullerenes and carbon nanotubes. Because of the electron-deficiency, fullerenes are reactive against dienes and can participate in the Diels–Alder reactions as dienophile [9, 10]. Recently, certain experimental and theoretical methods have been developed to functionalize the fullerenes, such as synthesis of C_{2v}(2)-$C_{78}Cl_6(C_5Cl_6)$ [11], synthesis of pentafluorosulfanyl-functionalized fullerenes [12], one-pot substitution of the twenty hydrogen atoms in pentagonal dodecahedrane ($C_{20}H_{20}$) by OH, F, Cl, and Br [13], functionalization of the C_{60} fullerene with metformin [14], the Diels-Alder reaction between C_{60} and acenes [15,16], functionalization of C_{20} with benzene [17], reaction of C_{60} with naphthalene [18] and cycloaddition reaction of C_{20} with pyrene [19]. The Diels-Alder and retro Diels-Alder reactions of the C_{60} fullerene with 9-hydroxy methylanthracene, 9-methoxy methylanthracene and bis(9-anthrylmethyl) adipate under solvent-free conditions were reported by Wang *et al.* [16]. It was found that the aforementioned reactions proceed with activation energies of 25.8, 21.8 and 24.9 kcal/mol, respectively. In another work, the kinetic studies were carried out on the Diels-Alder reaction of C_{60} with anthracene and tetracene [15].

Pyridine and pyrimidine are two basic heterocyclic compounds, which occur naturally within the structure of vitamins and natural products [20,21]. They also exist in the structure of many pharmaceutical agents such as antibacterial, antiviral, antioxidant, antidiabetic, anticancer, antimalarial and anti-inflammatory drugs [22-24]. Pyridine is widely used as a solvent as well as a precursor for the synthesis of various organic compounds. Since the flash point of pyridine is low, it is easily evaporated and dispersed in the air. It also dissolves in water, and consequently, its continuous release into the hydrosphere can be considered as a significant problem for human health and environment [25]. Therefore, the control and inactivation of pyridine in the environment can be important. Nanomaterials, which have a high surface to volume ratio, are very effective adsorbents for the removal of organic pollutants such as pyridine from the environment.

In the present study, the possibility of functionalization of the C_{20} fullerene with pyridine and pyrimidine was theoretically investigated in continuation of our previous works on various organic compounds [19, 26-28]. The important aims of this work are:
- To study the possibility of the functionalization of the C_{20} fullerene with pyridine and pyrimidine
- Investigation of the regioselectivity of the reactions
- Determining the frontier effective-for-reaction molecular orbitals (FERMOs) to describe the reactivity
- To study the charge transfer in transition states
- Determination of the synchronicity in the reactions

Computational methods
The geometries of the reactants, transition states and products were optimized at CAM-B3LYP/6-311G** level of the theory [29,30]. The optimized transition state structures were determined using the synchronous transit-guided quasi-Newton (STQN)

method [31]. The stationary points were characterized by frequency computations to verify that each transition state has only one imaginary frequency. The intrinsic reaction coordinates (IRC) calculations confirmed the TS structures [32, 33]. Single point energy calculations on the previously CAM-B3LYP/6-311G** optimized structures were performed using MP2/6-311G** level of theory [34]. All the calculations were performed using the Gaussian 09 chemical quantum software [35].

The values of the reactions rate constant k were calculated using the Eyring equation (1):

$$k = (\frac{K_B T}{h}) \exp(\frac{-\Delta G^{\ddagger}}{RT})$$ (1)

where K_B denotes the Boltzmann constant, T is the Kelvin temperature, h is Planck's constant, $\Delta G^{\ddagger}$ is the free energy of activation and R is the universal constant of gases [36].

The synchronicity (Sy) of the reactions was calculated using equation (2) [37]:

$$Sy = 1 - \frac{1}{2n\text{-}2} \sum \frac{|\delta B_i\text{-}\delta B_{av}|}{\delta B_{av}}$$ (2)

where δB_i is a relative variation of the bond index B_i at transition state, δB_{av} denotes a measure of the degree of progress for the transition state along the reaction path and n is the number of bonds that participate directly in the cycloaddition reaction. The numerical values for synchronicity (S_y) are variable from 0 to 1 for stepwise and concerted reactions, respectively. The bond index (B_i) and the atomic charges of the transition states were computed using natural bond orbital (NBO) analysis [38, 39].

The electrophilicity index (ω) was calculated using equation (3) [40]:

$$\omega = \frac{\mu^2}{2\eta}$$ (3)

where μ and η denote the chemical potential and chemical hardness, respectively.

Results and discussions
Optimization of the structures
In the first step of the study, ten possible reaction paths were considered between C$_{20}$ and the heterocyclic compounds, pyridine and pyrimidine. Figure 1 illustrates the considered reaction paths.
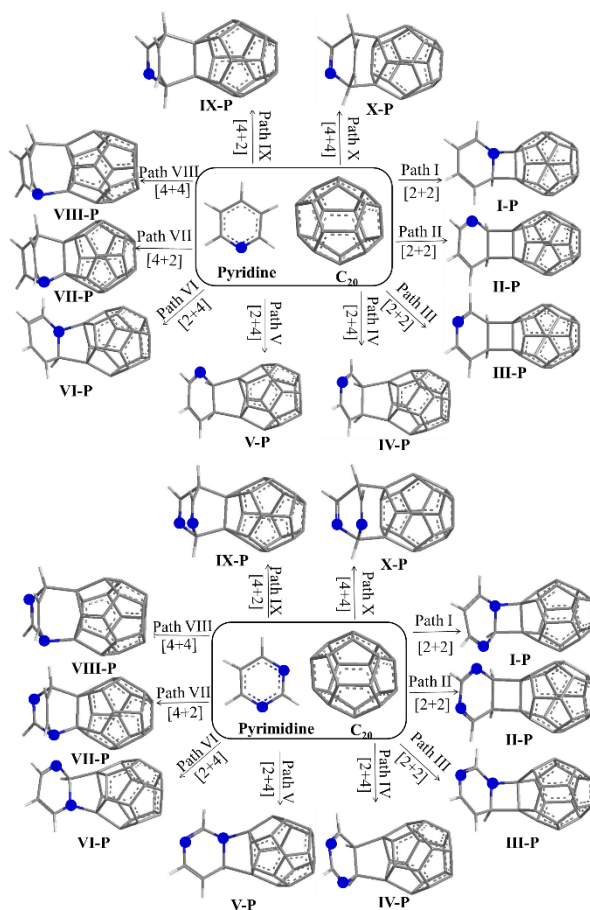
Figure 1. Ten possible reaction paths between C_{20} and pyridine as well as pyrimidine. The bullets represent the nitrogen atom in pyridine and pyrimidine.

According to Figure 1, three [2+2], two [4+4], three [2+4] and two [4+2] cycloaddition paths were considered. It is noteworthy that in the [2+4] and [4+2] cycloaddition paths, C_{20} acts as a diene and a dienophile, respectively. In all cases, different bonds of pyridine or pyrimidine participate in the cycloaddition reaction, which leads to the formation of various regio- or structural isomers.

At the next step, the geometries of the reactants (C_{20}, pyridine, and pyrimidine) and products were optimized using CAM-B3LYP/6-311G** method. To study the reactions, the transition states were calculated and detected. However, a true transition state was only detected for the [4+2] cycloaddition paths (VII and IX paths). More attempts to detect a true transition state for the other cycloaddition paths were unsuccessful. A similar trend has been also reported for the cycloaddition reaction between C_{20} and benzene [17]. The optimized structures of the reactants (C_{20}, pyridine and, pyrimidine), transition states and the products relevant to the VII and IX cycloaddition paths are given in Figure 2. The optimized geometries of the other products (**I-P**, **II-P**, **III-P**, **IV-P**, **V-P**, **VI-P**, **VIII-P**, and **X-P**) are given in Figures S1 and S2 of the supporting information.
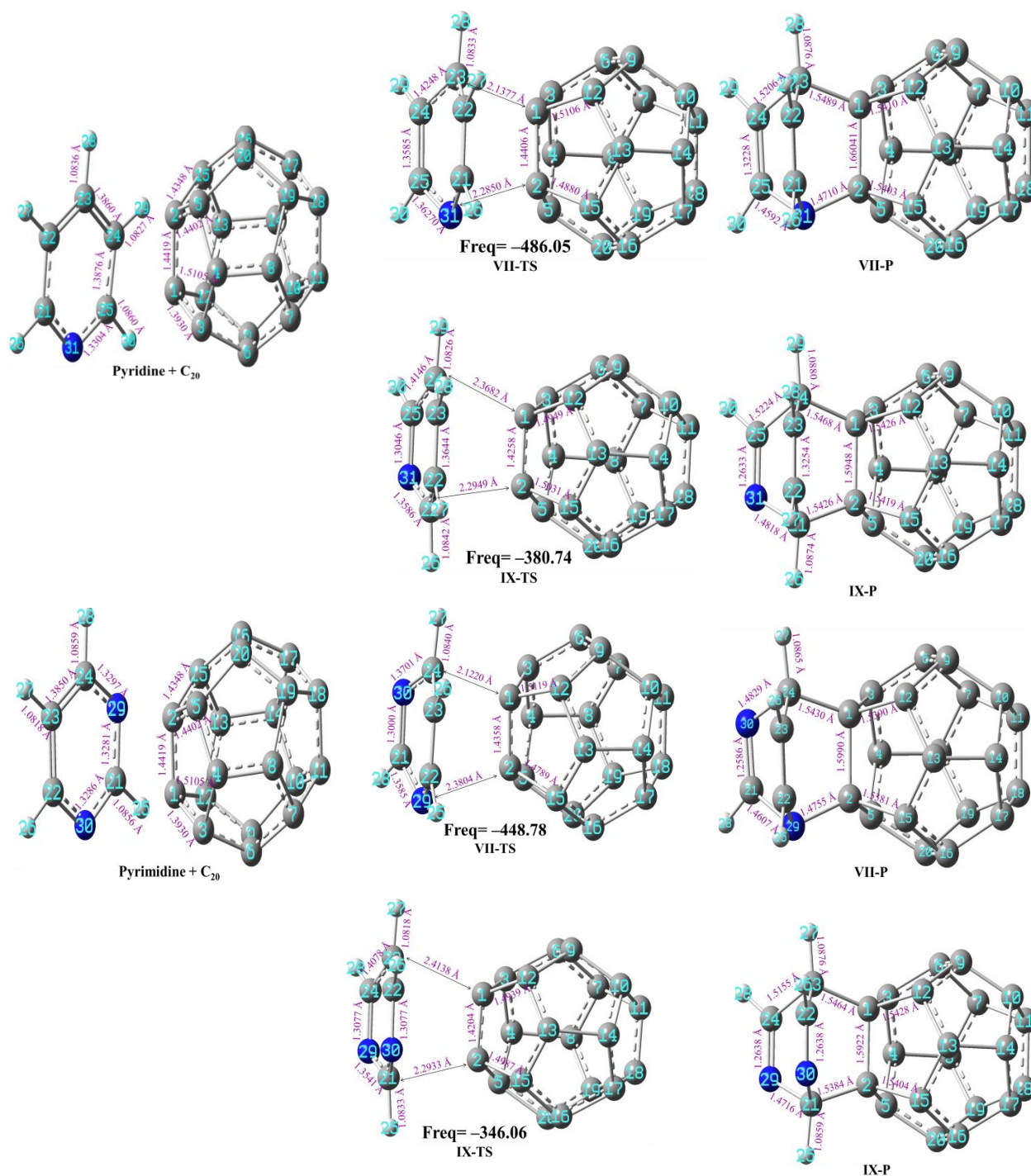
Figure 2. The optimized geometries of the reactants, transition states (along with their imaginary frequencies) and the products relevant to the cycloaddition reaction of the C$_{20}$ fullerene with pyridine (up) and pyrimidine (down)

Thermodynamic and kinetic parameters
Table S1, in the supporting information, lists the calculated values of the thermodynamic parameters (heats of formation; ΔH°_f, free energies of formation; ΔG°_f and entropies of formation; ΔS°_f), total energy (E_{tot}, obtained from MP2/6-311G** single point energy calculations), HOMO energies, LUMO energies, electrophilicity index (ω) and dipole moments for the reactants, transition states and products. To have more details over the PES of reaction, the thermodynamic parameters were computed for the reactants and products involved in all reaction paths. In addition, the kinetic parameters were calculated for the reaction paths VII and IX. Tables 1 and 2 summarize the calculated thermodynamic and kinetic parameters for reaction paths I to X.

Table 1. Calculated thermodynamic parameters (ΔH°_r and ΔG°_r in kJ.mol^{-1} and ΔS°_r in kJ.K^{-1}.mol^{-1}) and ΔE_{tot} (in a.u.) for the reaction paths between C_{20} and pyridine as well as pyrimidine.

Path[a]	ΔH°_r	ΔG°_r	ΔS°_r	ΔE_{tot}[c]	Path[b]	ΔH°_r	ΔG°_r	ΔS°_r	ΔE_{tot}[c]
I	-97.1	-32.7	-0.216	-0.0442	I	-113.1	-48.2	-0.218	-0.0473
II	-120.4	-55.9	-0.216	-0.0578	II	-120.8	-56.6	-0.215	-0.0568
III	-112.2	-48.3	-0.214	-0.0548	III	-109.6	-45.0	-0.217	-0.0477
IV	183.7	248.3	-0.217	0.0621	IV	173.6	238.3	-0.217	0.0598
V	172.9	237.9	-0.218	0.0585	V	228.1	292.0	-0.214	0.0900
VI	244.4	308.1	-0.214	0.0951	VI	221.9	285.6	-0.214	0.0916
VII	-118.6	-48.1	-0.236	-0.0545	VII	-138.2	-67.6	-0.237	-0.0606
VIII	108.7	179.5	-0.237	0.0396	VIII	96.8	167.7	-0.238	0.0368
IX	-192.1	-121.8	-0.236	-0.0856	IX	-205.2	-134.8	-0.236	-0.0887
X	30.3	101.1	-0.237	0.0037	X	29.9	100.9	-0.238	0.0061

[a,b] The data are relevant to the reactions of C_{20} with pyridine and pyrimidine, respectively.
[c] The results obtained from single point energy calculations using MP2/6-311G** method.

Table 2. The calculated values of the kinetic parameters ($\Delta H^{\ddagger \circ}$ and $\Delta G^{\ddagger \circ}$ in kJ.mol^{-1}, $\Delta S^{\ddagger \circ}$ in kJ.K^{-1}.mol^{-1} and $\Delta E^{\ddagger}_{tot}$ in a.u.) corresponding to the two reaction paths VII and IX

Path	$\Delta H^{\ddagger \circ}$	$\Delta G^{\ddagger \circ}$	$\Delta S^{\ddagger \circ}$	$\Delta E^{\ddagger}_{tot}$	k (s^{-1})
VII[a]	93.7	153.8	-0.202	0.0593	7.03×10^{-15}
IX[a]	48.7	107.6	-0.198	0.0374	8.73×10^{-7}
VII[b]	76.9	136.7	-0.201	0.0520	6.96×10^{-12}
IX[b]	41.7	100.6	-0.198	0.0352	1.47×10^{-5}

[a,b] The data are relevant to the reactions of C_{20} with pyridine and pyrimidine, respectively.
[c] The results obtained from single point energy calculations using MP2/6-311G** method.

Figures S3 and S4 in the supporting information show the IRC profile associated with the cycloaddition reactions between C_{20} and pyridine as well as pyrimidine. It is clear that all IRC profiles confirm the corresponding transition states.

To evaluate the reaction paths in a more comparable manner, relative free energies are plotted along a diagram and are shown in Figure 3. The diagrams corresponding to the heats of formation and total energies are given in Figure S5 of the supporting information.

Analysis of the results indicates that:

1) Due to the negative values of ΔH°_r and ΔG°_r, the reaction paths I, II, III, VII, and IX are possible thermodynamically. On the other hand, the reaction paths IV, V, VI, VIII, and X are undesirable.

2) Both reaction entropies (ΔS°_r) and activation entropies ($\Delta S^{\ddagger \circ}$) are reduced, which can be attributed to the diminution the freedom degrees of the reactants during the ring closure.

3) The activation free energy $\Delta G^{\ddagger \circ}$ corresponding to the reaction path **IX** is less than that for **VII** one, which indicates that the former path is kinetically more favorable than the later. Also, it can be concluded that path **IX**, which takes place via formation of two new C–C bonds between two fragments, is more favorable than path **VII** which occurs *via* formation of two different bonds,

C–C and C–N. Accordingly, the favorable formation of **IX-P** adduct compared to the **VII-P** one can be attributed to the easier formation of C–C bond rather than C–N one.

4) Analysis of the electrophilicity index (ω) in the reactants indicates that C_{20} is more electrophilic than pyridine as well as pyrimidine and consequently, it can be concluded that electron density is fluxed from the heterocyclic compound toward C_{20}.

5) The calculated dipole moments relevant to the products show that the polarity is increased dramatically when the fullerene is functionalized with the nitrogen-containing compounds.

6) A good agreement is observed between the results obtained from CAM-B3LYP/6-311G** method and those obtained from MP2/6-311G** single point calculations (Figure S5).

A comparison between the aforementioned results with those reported for the benzene [17] reveals that the cycloaddition reaction between C_{20} and benzene is relatively faster than between C_{20} and pyridine or pyrimidine.
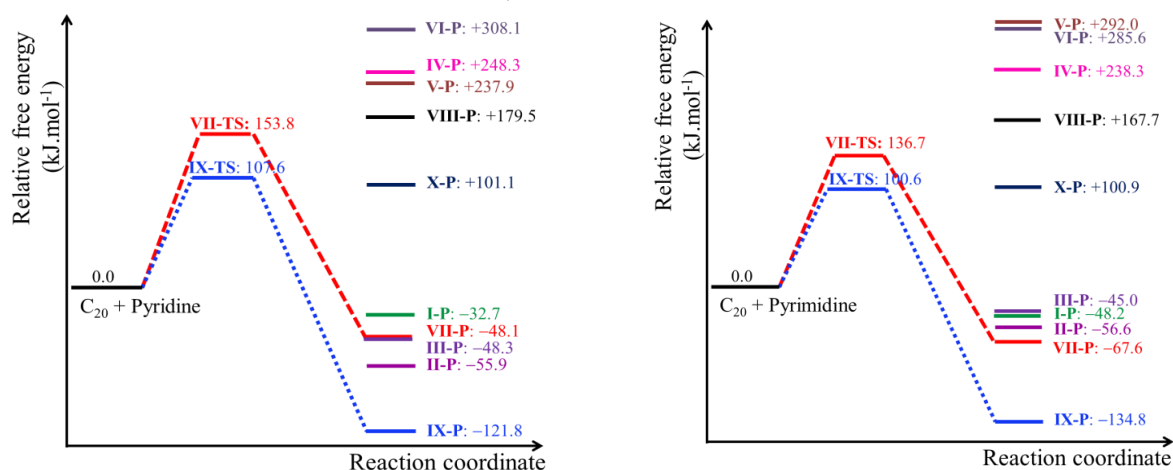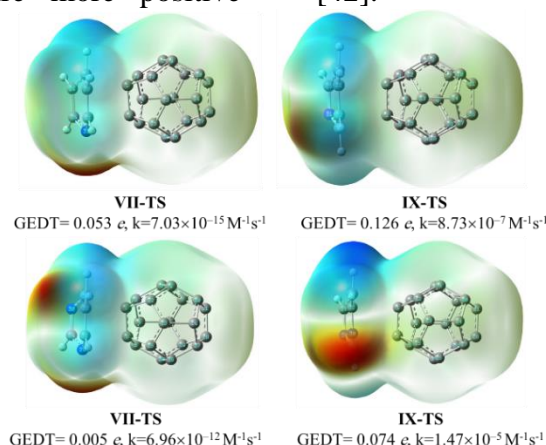
Figure 3. Free energies diagrams for reaction paths between C_{20} and pyridine as well as pyrimidine

Global electron density transfer at transition states

Global electron density transfer (GEDT) is one of the important factors in most organic reactions. This factor is often one of the characteristics of transition states in cycloaddition reactions and sometimes determines the energy barriers [41]. Thus, in the next phase of the study, the GEDT values were calculated for **VII** and **IX** reaction paths using NBO analysis. Figure 4 illustrates the calculated values of the GEDTs along with the molecular electrostatic potential (MESP) map for the transition states. In the MESP map, the blue regions are more positive having lesser electron density and the red ones are more negative and have greater electron density.

Analysis of the results presented in Figure 4 shows that C_{20} acts as an electron acceptor. It is also clear that the transition state **IX-TS** is more polar than **VII-TS** one. In addition, the GEDT value for **IX-TS**, the transition state of the faster reaction path, is larger than that for **VII-TS**. A similar trend is also observed for the reaction between pyrimidine and C_{20}. The aforementioned results show that C_{20} is an electron-deficient molecule and tend to reacts with electron-rich compounds [42].

VII-TS
GEDT= 0.053 e, k=7.03×10^{-15} M^{-1}s^{-1}

IX-TS
GEDT= 0.126 e, k=8.73×10^{-7} M^{-1}s^{-1}

VII-TS
GEDT= 0.005 e, k=6.96×10^{-12} M^{-1}s^{-1}

IX-TS
GEDT= 0.074 e, k=1.47×10^{-5} M^{-1}s^{-1}

Figure 4. The molecular electrostatic potential (MESP) map and the global electron density transfer (GEDT) values for the transition states. The blue and red colors refer to the regions with low and high electron density, respectively.

Interaction of the frontiers molecular orbitals

To study the interaction of the frontier orbitals, the energy differences between the frontier orbitals of the electron donor fragments, pyridine or pyrimidine, and the electron acceptor fragment, C_{20}, were calculated. The results indicated that the $HOMO_{Pyr}$–$LUMO_{Ful}$ energy difference, 0.2314 a.u., is less than that for $HOMO_{Ful}$–$LUMO_{Pyr}$ one, 0.2651 a.u. (Figure S6). A similar trend is also observed for the energy differences between the fr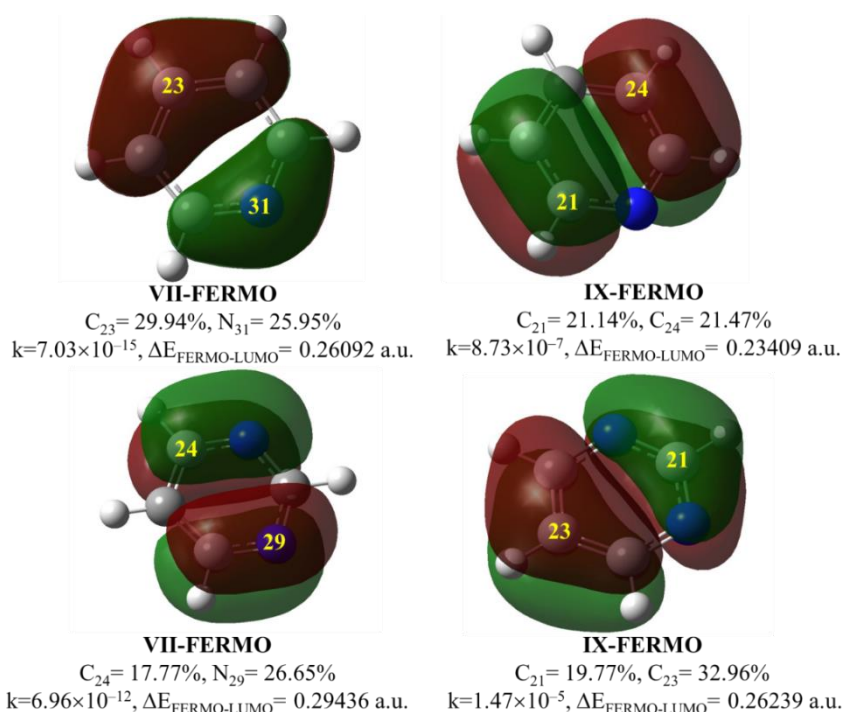ontier orbitals of pyrimidine and fullerene (Figure S6). Accordingly, the interaction between the HOMO of pyridine or pyrimidine and the LUMO of C_{20} is more favorable than the other alternative interaction (Figure S6).

The HOMO-LUMO interactions between reactants always do not work accurately. Besides, the estimating when their interactions are appropriate is difficult. Recently, FERMO (Frontier Effective-for-Reaction Molecular Orbitals) concept has been introduced to describe the reactivity of the different active sites of a reactant [43]. The FERMO concept considers a

frontier molecular orbital, HOMO or another occupied molecular orbital near to the HOMO, in which the active sites have a large contribution therein. It has been approved that the FERMOs can work better than HOMO in many reactions. It should be here noted that the FERMO concept is used only for description the reactivity of different active sites in a molecule and not for comparison the reactivity of different molecules. We applied this concept satisfactorily to describe the reactivity of the different active sites of pyrene [19]. Therefore, to achieve a better description for the interactions between the frontier orbitals, the relative participation of the active sites of pyridine (C$_{21}$, C$_{23}$, C$_{24}$, and N$_{31}$ atoms) and pyrimidine (C$_{21}$, C$_{23}$, C$_{24}$, and N$_{29}$ atoms) were calculated in their different occupied molecular orbitals. Then, the

FERMO orbital was determined in terms of the maximum contribution of the active sites in the occupied molecular orbital. The FERMOs of pyridine and pyrimidine participating in the reaction paths VII and IX are given in Figure 5. In addition, the energy difference between each FERMO of the heterocycle and the LUMO of the C$_{20}$ fullerene are given in Figure 5. The comparison between the reactions rate constant and the FERMO-LUMO gap, presented in Figure 5, indicates that FERMO concept can describe the reactivity of the active sites of pyridine and pyrimidine against C$_{20}$. Therefore, the favored reaction path is IX for both heterocyclic compounds because there is a smaller energy difference between the FERMO of the heterocycle and the LUMO of the fullerene.

VII-FERMO
C$_{23}$= 29.94%, N$_{31}$= 25.95%
k=7.03×10^{-15}, $\Delta E_{\text{FERMO-LUMO}}$= 0.26092 a.u.

IX-FERMO
C$_{21}$= 21.14%, C$_{24}$= 21.47%
k=8.73×10^{-7}, $\Delta E_{\text{FERMO-LUMO}}$= 0.23409 a.u.

VII-FERMO
C$_{24}$= 17.77%, N$_{29}$= 26.65%
k=6.96×10^{-12}, $\Delta E_{\text{FERMO-LUMO}}$= 0.29436 a.u.

IX-FERMO
C$_{21}$= 19.77%, C$_{23}$= 32.96%
k=1.47×10^{-5}, $\Delta E_{\text{FERMO-LUMO}}$= 0.26239 a.u.

Figure 5. The FERMOs of pyridine and pyrimidine for the reaction paths VII and IX, the participation of the active sites in MOs, the values of the reactions rate constants and the FERMO$_{\text{Het}}$-LUMO$_{\text{Ful}}$ gap

Determination of the synchronicity
The cycloaddition reactions often take place *via* a concerted mechanism. Therefore, to study the synchronicity of

the reaction paths, the numerical value of synchronicity (*Sy*) was calculated from the variation of the bond index in each transition state.

For a selected bond i, its bond index B_i was calculated in the reactants (B_i^R), transition state (B_i^{TS}) and product (B_i^P) from Wiberg bond index obtained from NBO calculations. Then, the relative variation of the bond index at the transition state δB_i was calculated using equation (4).

$$\delta B_i = \frac{(B_i^{TS} - B_i^R)}{(B_i^P - B_i^R)} \qquad (4)$$

The average of all δB_is obtained (δB_{av}) which is a measure of the degree of progress for the transition state along the reaction path. Finally, the synchronicity was calculated using equation (2) [37]. The results are given in Table 3.

The results presented in Table 3 indicate that the reaction paths are relatively synchronous. The synchronicity value for the reaction path IX is greater than that for VII one. It is noteworthy that the IX path, which takes place *via* the formation of two similar C–C bonds between diene and dienophile, is slightly more synchronous than the reaction path VII, which occurs *via* formation of two different bonds, C–C and C–N. Thus, it can be concluded that the formation of two similar bonds in a cycloaddition reaction leads to slightly more synchronicity.

Conclusion

In this work, the possibility of the functionalization of the C_{20} fullerene with pyridine and pyrimidine was investigated, theoretically. The results revealed that the most effective cycloaddition reactions are two [4+2] paths, in which the fullerene acts as a dienophile. It was also found that a [4+2] reaction path in which C_{20} reacts with pyridine or pyrimidine *via* formation of two C–C bonds is more favorable than the reaction that occurs *via* formation of two different bonds, C-C and C–N. The favorable reaction paths for pyridine and pyrimidine occur with the rate constant of 8.73×10^{-7} and 1.47×10^{-5} s^{-1} at 25 °C, respectively. The calculation of the global electron density transfer (GEDT) and the molecular electrostatic potential (MESP) map showed that the transition states are slightly polar and electron density is fluxed from pyridine or pyrimidine toward the fullerene. The FERMO concept can describe the reactivity of the different active sites in the pyridine and pyrimidine. The synchronicity values of the reactions were also calculated and the results showed that the reactions are relatively synchronous.

Table 3. The calculated values of the synchronicity (Sy) for the reactions of C_{20} with pyridine and pyrimidine.

Path VII[a]	δB_{C1-C2}	δB_{C1-C23}	$\delta B_{C23-C24}$	$\delta B_{C24-C25}$	$\delta B_{C25-N31}$	δB_{C2-N31}	δB_{av}	Sy
	0.2973	0.4022	0.4609	0.3371	0.3480	0.2824	0.3547	0.9133
Path IX[a]	δB_{C1-C2}	δB_{C1-C24}	$\delta B_{C24-C25}$	$\delta B_{C25-N31}$	$\delta B_{C21-N31}$	δB_{C2-C21}	δB_{av}	Sy
	0.2067	0.2646	0.3434	0.2746	0.3328	0.2862	0.2847	0.9240
Path VII[b]	δB_{C1-C2}	δB_{C1-C24}	$\delta B_{C24-N30}$	$\delta B_{C21-N30}$	$\delta B_{C21-N29}$	δB_{C2-N29}	δB_{av}	Sy
	0.2911	0.3923	0.4385	0.3163	0.3209	0.2299	0.3315	0.8987
Path IX[b]	δB_{C1-C2}	δB_{C1-C23}	$\delta B_{C23-C24}$	$\delta B_{C24-N29}$	$\delta B_{C21-N29}$	δB_{C2-C21}	δB_{av}	Sy
	0.1804	0.2363	0.2895	0.2438	0.3117	0.2670	0.2548	0.9185

[a,b] The data are relevant to the reactions of C_{20} with pyridine and pyrimidine, respectively.

Abbreviations
Ful: fullerene
Pyr: pyridine
Pyrm: pyrimidine
Het: heterocycle

References
[1] H.W. Kroto, J.R. Heath, S.C. O'Brien, R.F. Curl, R.E. Smalley, *Nature*, **1985**, *318*, 162-163.

[2] M. Eslami Moghadam, A. Abolhosseini Shahrnoy, T. Karimi, S. Alyar, *Iran. Chem. Commun.*, **2016**, *4*, 115-122.

[3] H. Prinzbach, A. Weiler, P. Landenberger, F. Wahl, J. Wörth, L.T. Scott, M. Gelmont, D. Olevano, B.V. Issendorff, *Nature*, **2000**, *407*, 60-63.

[4] B.L. Zhang, C.H. Xu, C.Z. Wang, C.T. Chan, K.M. Ho, *Phys. Rev. B*, **1992**, *46*, 7333-7336.

[5] S.D. Oosterhout, V. Savikhin, J. Zhang, Y. Zhang, M.A. Burgers, S.R. Marder, G.C. Bazan, M.F. Toney, *Chem. Mater.*, **2017**, *29*, 3062-3069.

[6] T. Umeyama, H. Imahori, *J. Mater. Chem. A*, **2014**, *2*, 11545-11560.

[7] N. Martín, T. Da Ros, J.-F. Nierengarten, *J. Mater. Chem. B*, **2017**, *5*, 6425-6427.

[8] F.Y. Hsieh, A.V. Zhilenkov, I.I. Voronov, E.A. Khakina, D.V. Mischenko, P.A. Troshin, S.H. Hsu, *ACS Appl. Mater. Interfaces*, **2017**, *9*, 11482-11492.

[9] F. Cataldo, D.A. García-Hernández, A. Manchado, *Fullerenes, Nanotubes, Carbon Nanostruct.*, **2015**, *23*, 818–823.

[10] T. Yang, R. Fukuda, R. Cammi, M. Ehara, *J. Phys. Chem. A*, **2017**, *121*, 4363–4371.

[11] C. Gao, L. Abella, H.-R. Tian, X. Zhang, Y.-Y. Zhong, Y.-Z. Tan, X.-Z. Wu, A. Rodríguez-Fortea, J.M. Poblet, S.-Y. Xie, R.-B. Huang, L.-S. Zheng, *Carbon*, **2018**, *129*, 286-292.

[12] S.-Y. Qing, N.J. DeWeerd, A.V. Matsnev, S.H. Strauss, J.S. Thrasher, O.V. Boltalina, *J. Fluorine Chem.*, **2018**, *211*, 52-59.

[13] F. Wahl, A. Weiler, P. Landenberger, E. Sackers, T. Voss, A. Haas, M. Lieb, D. Hunkler, J. Wçrth, L. Knothe, H. Prinzbach, *Chem. Eur. J.*, **2006**, *12*, 6255-6267.

[14] H. Veisi, R. Masti, D. Kordestani, M. Safaei, O. Sahin, *J. Mol. Catal. A Chem.*, **2014**, *385*, 61-67.

[15] G.H. Sarova, M.N. Berberan-Santos, *Chem. Phys. Lett.*, **2004**, *397*, 402-407.

[16] G.W. Wang, Z.X. Chen, Y. Muratac, K. Komatsu, *Tetrahedron*, **2005**, *61*, 4851-4856.

[17] S.A. Siadati, N. Nami, *Physica E*, **2016**, *84*, 55-59.

[18] X. Cheng, A.T. Kan, M.B. Tomson, *J. Chem. Eng. Data*, **2004**, *49*, 675-683.

[19] M. Soleymani, H.D. Khavidaki, *Comp. Theor. Chem.*, **2017**, *1112*, 37-45.

[20] P. Kiuru, J. Yli-Kauhaluoma, *Heterocycles in natural product synthesis*, Wiley-VCH Verlag GmbH & Co. KGaA, **2011**, Chap. 8, P. 267-297.

[21] W. Xiang, S. Choudhary, E. Hamel, S.L. Mooberry, A. Gangjee, *Bioorg. Med. Chem.*, **2018**, *2*, 2437-2451.

[22] A. Nakhaei, A. Davoodnia, S. Yadegarian, *Iran. Chem. Commun.*, **2018**, *5*, 334-345.

[23] R.D. Taylor, M. MacCoss, A.D.G. Lawson, *J. Med. Chem.*, **2014**, *57*, 5845-5859

[24] A.A. Ghoneim, M.G. Assy, E.K. Mohamed, I. Ragab, *Iran. Chem. Commun.*, **2017**, *5*, 195-206.

[25] H. Xu, X. Zhang, Y. Zhang, *Environ. Technol*., **2018**, *39*, 1470-1480.

[26] M. Soleymani, *Monatshe. Chem. Chem. Mon.*, **2018**, *149*, 2183–2193.

[27] M. Soleymani, *Theor. Chem. Acc.*, **2019**, *138*, 87.

[28] M. Soleymani, *Struct. Chem.*, **2019**, *30*, 1173-1184.

[29] AT. Yanai, D. Tew, N. Handy, *Chem. Phys. Lett.*, **2004**, *393*, 51-57.

[30] A.D. McLean, G.S. Chandler, *J. Chem. Phys.*, **1980**, *72*, 5639-5648.

[31] C. Peng, P.Y. Ayala, H.B. Schlegel, M.J. Frisch, *J. Comput. Chem.*, **1996,** *17*, 49-56.

[32] C. Gonzalez, H.B. Schlegel, *J. Chem. Phys.*, **1989**, *90*, 2154-2161.

[33] C. Gonzalez, H.B. Schlegel, *J. Phys. Chem.*, **1990**, *94*, 5523-5527.

[34] M. Head-Gordon, T. Head-Gordon, *Chem. Phys. Lett.*, **1994**, *220*, 122-128.

[35] M.J. Frisch, *et al.*, Gaussian 09, Revision A. 02, Gaussian Inc,. Wallingford, CT, **2009**.

[36] H. Eyring, *J. Chem. Phys.*, **1935**, *3*, 107-115.

[37] B. Lecea, A. Arrieta, G. Roa, J.M. Ugalde, F.P. Cossio, *J. Am. Chem. Soc.*, **1994**, *116*, 9613-9619.

[38] A.E. Reed, L.A. Curtiss, F. Weinhold, *Chem. Rev.*, **1988**, *88*, 899-926.

[39] J.E. Carpenter, F.J. Weinhold, *J. Mol. Struct.*, **1988**, *169*, 41-62.

[40] R.G. Parr, L.V. Szentpaly, S. Liu, *J. Am. Chem. Soc.*, **1999**, *121*, 1922-1924.

[41] L.R. Domingo, *RSC Adv.*, **2014**, *4*, 32415-32428.

[42] F. Wudl, A. Hirsch, K.C. Khemani, T. Suzuki, P.M. Allemand, A. Koch, H. Eckert, G. Srdanov, H.M. Webb, *ACS Symp. Ser.*, **1992**, *481*, 161-175.

[43] F.A. La Porta, T.C. Ramalho, R.T. Santiago, M.V.J. Rocha, E.F.F. da Cunha, *J. Phys. Chem. A*, **2011**, *115*, 824-833.